arXiv:1301.3018v1 [physics.atom-ph] 14 Jan 2013

Non-destructive Faraday imaging of dynamically controlled ultracold atoms

Miroslav Gajdacz, Poul L. Pedersen, Troels Mørch, Andrew J. Hilliard, Jan Arlt, and Jacob F. Sherson[a)]
Danish National Research Foundation Center for Quantum Optics, Institut for Fysik og Astronomi, Aarhus Universitet, Ny Munkegade 120, 8000 Aarhus C, Denmark.

(Dated: 15 January 2013)

We introduce an easily implementable method for non-destructive measurements of ultracold atomic clouds based on dark field imaging of spatially resolved Faraday rotation. The dependence on laser detuning, atomic density and temperature is characterized in a detailed comparison with theory. Due to low destructiveness, the same cloud can be imaged up to 2000 times. The technique is applied to avoid the effect of shot-to-shot fluctuations in atom number calibration, to demonstrate single-run vector magnetic field imaging and single-run spatial imaging of the system's dynamic behavior. This paves the way towards quantum state engineering using feedback control of ultracold atoms.

One of the most fundamental features of quantum mechanics is the appearance of intrinsically non-classical effects induced by measurements. An important class of measurements for creating quantum technologies is that of quantum-non-demolition (QND) measurements. In particular, QND measurements followed by feedback allow the deterministic production of useful quantum states[1].

Non-destructive measurements of atomic ensembles have been realized using several dispersive techniques such as phase contrast imaging (PCI)[2], polarization spectroscopy using Faraday rotation (FR)[1,3], diffractive techniques[4], and most recently, partial-transfer absorption imaging[5]. The achievable signal-to-noise ratio in all of these approaches is similar and hence experimental requirements typically prescribe the method of choice.

QND measurements based on FR in room temperature atomic ensembles have been used to demonstrate entanglement[6], quantum memory[7], and quantum teleportation[8]. In the regime of cold atoms[9,10], this approach has yielded spectacular results including spin squeezing[11], magnetometry[12], and the observation of many-body dynamics[13].

In this Letter, we present a non-destructive imaging technique for ultracold atomic samples based on Faraday rotation. The technique is straightforward to implement in existing experiments and provides valuable diagnostic tools for the research directions outlined above. Faraday imaging is based on the polarization rotation that occurs when light passes through a spin-polarized atomic sample. In our approach, the spatially dependent angle of rotation is detected by measuring the intensity of rotated light transmitted through a polarizer on a camera. The method can thus be regarded as a form of dark field imaging[2] and we refer to it as dark field Faraday imaging (DFFI). It is considerably simpler to implement than PCI and dual-port homodyne detection schemes[10], and can be realized by inserting a single polarizer in a standard absorption imaging set-up. We show that DFFI allows for precise measurements over a wide range of atomic densities and temperatures. The detuning dependence of the method and its destructive effects on the atomic sample are evaluated in a detailed comparison with theory. Furthermore, we demonstrate multiple probing of ultracold atoms with up to 2000 images per experimental cycle. This allows for a number of diagnostic applications, including the determination of ambient vector magnetic fields or of dynamically controlled trapping frequencies in a single experimental run. In addition, we demonstrate a reduction of the deleterious effects of shot-to-shot atom number fluctuations by rescaling absorption measurements with Faraday images. These applications show that DFFI provides a valuable tool in modern ultracold atom experiments.

Faraday rotation can be described using a model of the dispersive light-matter interaction[1]. The polarization rotation arises from the vector term of the scattering Hamiltonian

$$\hat{H}^{(\mathrm{vec})} = g \sum_{f'} \frac{\alpha^{(\mathrm{vec})}_{f,f'}}{\Delta_{f,f'}} \hat{F}_z \left(\hat{N}_+ - \hat{N}_- \right) /2, \qquad (1)$$

where $\hat{F}_z$ is the z-component of the collective atomic angular momentum (defined by the direction of light propagation). $\hat{N}_\pm$ are photon number operators for the two cir-

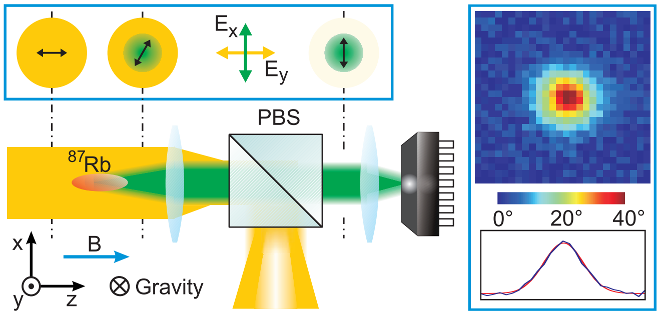

FIG. 1. Sketch of the Faraday imaging system and a resulting image (right) at $T = 1.5\ \mu$K and $N = 10^6$ atoms. The polarization of the light is indicated (top) by displaying cross sections of the imaging beam obtained from a rotation around the dash-dot lines.

[a)] sherson@phys.au.dk

cular polarizations, $\alpha^{(\mathrm{vec})}_{f,f'}$ is the vector polarizability of a given atomic transition, $\Delta_{f,f'} = \omega - \omega_{f,f'}$ is the probe detuning with respect to that transition and $g = \omega/(2\epsilon_0 V)$, where V is the volume of the atomic sample. The Hamiltonian yields eigenvalues for left and right handed polarized light that are different in sign and magnitude, so that the linear polarization of the incident light is rotated. Since the atom number N_{at} is large and all atoms are in the same internal state with average z-axis projection of the angular momentum $\langle \hat{f}_z \rangle$, we can treat the collective angular momentum classically and use $\hat{F}_z = N_{\mathrm{at}} \langle \hat{f}_z \rangle$. To account for the spatial variation of the density, we substitute $N_{\mathrm{at}}/V \to \rho(\mathbf{r})$.

In our experiments, atoms are prepared in the $|f = 2, m_f = 2\rangle$ state of ^{87}Rb, and for imaging wavelengths close to the D2 line, the spatially resolved Faraday angle is given by

$$\theta_F(x, y) = \frac{\langle \hat{f}_z \rangle \Gamma \lambda^2}{16\pi \Delta_{\mathrm{eff}}} \int \rho(\mathbf{r}) dz = c_F(\Delta_{\mathrm{eff}}) \tilde{\rho}(x, y), \qquad (2)$$

where Γ is the natural linewidth, λ is the wavelength of the imaging light and the effective detuning is given by

$$\frac{1}{\Delta_{\mathrm{eff}}} = \frac{1}{20} \left(\frac{28}{\Delta_{2,3}} - \frac{5}{\Delta_{2,2}} - \frac{3}{\Delta_{2,1}} \right). \qquad (3)$$

Thus, the spatially dependent angle of polarization is given by a product of the Faraday coefficient $c_F(\Delta_{\mathrm{eff}})$ and the column density of the sample $\tilde{\rho}(x, y)$.

Figure 1 schematically shows the experimental setup to measure this angle of polarization. When a beam of linearly polarized light impinges on a cloud of magnetically oriented atoms, a spatial rotation pattern is imprinted on the beam. The polarization pattern is collimated and the two linear components are subsequently separated on a polarizing beam splitter (PBS). The polarization of the imaging beam is chosen such that its transmission through the PBS is minimized in the absence of atoms. A second lens then forms an image in the detection system, which contains a mask to allow for partial readout and thereby high frame rates in an Electron Multiplying Charge Coupled Device (EMCCD) camera. This camera enables low light intensity imaging and hence reduces measurement destructiveness, which is crucial for repeated probing and feedback experiments.

To reconstruct the rotation angle, we require the intensities of the incoming and the rotated light. In principle, this can be achieved by measuring the intensity of the light reflected by the PBS. In our realization, however, we avoid the necessary cross-calibration by making use of the experimental imperfection of the PBS, which leads to a finite transmission of non-rotated light. Thus, images without atoms can be used to determine the incoming light intensity and compensate for beam profile inhomogeneity. We measure the cube suppression $\mathrm{CS} = \mathrm{P_{min}}/\mathrm{P_{max}} = 1.5 \cdot 10^{-3}$ as the ratio of minimum to maximum power transmitted through the PBS. The transmitted light intensity is hence given by $I = I_{\mathrm{min}}(\mathrm{CS}\cos^2\theta_{\mathrm{F}} + \sin^2\theta_{\mathrm{F}})/\mathrm{CS}$, where I_{min} is the intensity without atoms. The rotation angle is obtained from

$$\sin^2\theta_F = \left(\frac{I}{I_{\mathrm{min}}} - 1 \right) \left(\frac{\mathrm{CS}}{1 - \mathrm{CS}} \right). \qquad (4)$$

Absolute light intensity calibration is therefore not required to evaluate the rotation angle as long as the EMCCD camera has a linear response.

The Faraday imaging technique requires light detuned from atomic resonance by $\sim 100\Gamma$. This light is produced by an extended cavity diode laser locked to a reference laser via a tunable offset lock[14]. Since the $f = 2 \to f' = 3$ transition has the highest oscillator strength (Eq. (3)), we use $\Delta_{2,3} \equiv \Delta$ as a measure of the laser detuning. This setup allows us to lock the laser in the range $\Delta = (-1.5, 1.8)$ GHz and to adjust the detuning dynamically in a single run within a range of 0.7 GHz. The imaging light pulses are produced by an acousto-optic modulator.

The experiments using DFFI are performed in the following sequence. Ultracold clouds of ^{87}Rb atoms in the $|f = 2, m_f = 2\rangle$ state are produced by forced radio frequency evaporation in a magnetic trap[15] with typical axial and radial trapping frequencies of $\omega_z = 2\pi \cdot 17$ Hz and $\omega_r = 2\pi \cdot 192$ Hz respectively. The temperature and number of atoms in the cloud is adjusted by tailoring the evaporation sequence appropriately. The Faraday imaging light propagates along the symmetry axis (z-axis in Fig. 1) of the cigar-shaped trap, corresponding to the magnetic field direction. At the end of each experimental sequence, we acquire a time-of-flight absorption image. This provides an independent measurement of the number of atoms and the temperature of the cloud. The atom number calibration is crucial for the quantitative comparison of experiment and theory and is discussed in more detail below.

It is of great importance to confirm that DFFI can precisely measure relevant properties of the atomic clouds. We first investigate the Faraday coefficient c_F as a function of the laser detuning. Figure 2 a) shows this dependence, where $c_F = \theta^{\mathrm{sum}}/N_{\mathrm{abs}}$ is obtained experimentally by summing θ_F (obtained from Eq. (4)) over all CCD pixels and N_{abs} is the atom number obtained from the absorption image. We focus on the characterization of the blue detuned side, to avoid complications arising from molecular resonances[10]. In each experimental sequence, we prepared a thermal cloud at 3 μK and took 35 Faraday images of 1 μs duration separated by 4.7 ms; each pulse had 160 μW and the laser detuning was swept over 700 MHz. The data agrees well with the theoretical value up to an overall scaling factor of 0.64. We ascribe this discrepancy to the spatial inhomogeneity in the magnetic potential and systematic calibration effects[16]. Nonetheless, the agreement is good in light of previous work[9,10] and justifies neglecting the tensor terms in Eq. (1) which would have induced detuning dependent corrections.

The destructiveness of DFFI is of similar importance.

We measured it at four different detunings by exposing the cloud to Faraday light for various durations and subsequently measuring the resulting temperature in absorption images. To obtain the scattering rate from the cloud temperature, we assume that each scattering event transfers twice the photon recoil energy and the heat capacity of an atom is $\frac{3}{2}k_B$. The measured scattering rate shown in Fig. 2 a) is consistent with theory to within 15%. Figure 2 a) also illustrates that the scattering rate decays as $1/\Delta^2$ whereas the Faraday coefficient falls off as $1/\Delta$. This well known difference is the key feature for the non-destructiveness of the method.

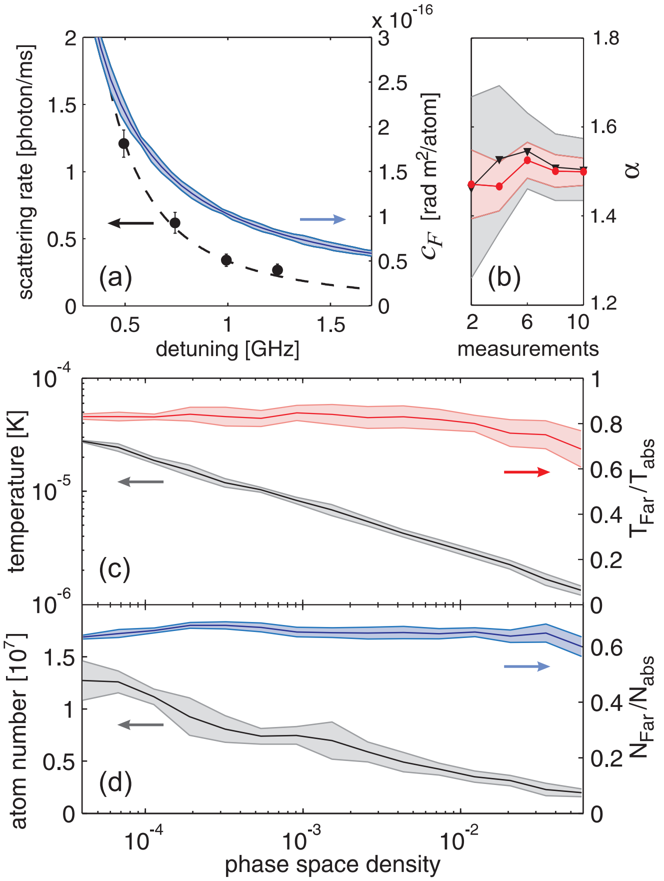

FIG. 2. Characterization of DFFI. a) Faraday coefficient c_F and photon scattering rate as a function of the detuning. b) Absorption image calibration factor α depending on the number of measurements with (dots) and without (triangles) Faraday scaling. c), d) Temperature and atom number obtained from DFFI compared to results from absorption imaging. Arrows in the figures indicate the appropriate axes.

To investigate the measurement precision, we employ DFFI at different times in the evaporation sequence, sampling an atom number range from $1.5 \cdot 10^7$ to $1.6 \cdot 10^6$ and a temperature range from 30 μK to 1 μK. The upper and lower limits of this range are set by the EMCCD size and the magnification of the detection system. In each experimental sequence, 20 Faraday images are taken, out of which the first six contain atoms and an average of the rest provides the intensity reference $I_{\min}$. The pulse parameters correspond to those in Fig. 2 a) at detuning +750 MHz, leading to an absorption probability per DFFI pulse of $6 \cdot 10^{-4}$. The measured temperatures and atom numbers are shown in Fig. 2 c) and d) as a function of phase space density. In both cases DFFI allows for precise measurements over the entire parameter range, despite the fact that the atom number and temperature are changed dramatically. To verify the accuracy of these measurements, we have taken a calibrated absorption image[17] at the end of each experimental sequence. Figures 2 c) and d) show that the proportionality factor between the two methods is essentially constant. It is 0.82(9) for the temperature, which represents good agreement considering the previously mentioned systematic effects in both methods. Consistent with the results in Fig. 2 a), the atom number proportionality factor is 0.65(3). This result confirms that DFFI provides precise non-destructive measurements and good accuracy can be obtained by appropriate scaling of the results.

Having established the functionality of the method, we turn to the first application of DFFI. We demonstrate a reduction of the deleterious effects of shot-to-shot fluctuations in an ultracold atomic sample. In general creating a source of ultra-cold atoms with a reproducible atom number is a notoriously difficult experimental task. Our method supplements previous experiments[5,18,19] that used non-destructive measurements to compensate for atom-number fluctuations. Here, we use DFFI to shorten the key experimental task of calibrating absorption imaging. In the state of the art method[17], the scattering cross section is scaled by a factor α, obtained by acquiring absorption images at various light intensities. Due to shot-to-shot fluctuations, tens of measurements are typically required to obtain a good estimate of α. Here, we repeat the procedure but add a DFFI pulse in each sequence to scale the obtained atom number. Figure 2 b) shows α as a function of the number of sampled light intensities both with and without the Faraday scaling. Since scaling with DFFI avoids shot-to-shot fluctuations, a good estimate can be obtained with considerably fewer experimental repetitions; in fact, two are sufficient in our case.

Due to the magnetic field dependence of the Faraday effect, DFFI also allows for new avenues in magnetometry. Vapor cell optical magnetometers[20] have been extremely successful, reaching sensitivities competitive with state of the art SQUID magnetometers and allow for both spatial resolution[21] and vector field magnetometry[22]. Cold and ultracold atoms hold the promise for further improvement of the precision due to the reduced thermal motion. Spatially resolved magnetometry has been realized in these systems[12,23,24] and recently vector magnetometers were explored[25,26]. In this work, we take an important conceptual step further in this direction by realizing a single shot vector magnetometer based on ultracold atoms in an optical lattice. In principle, this method allows for spatially resolved magnetometry down

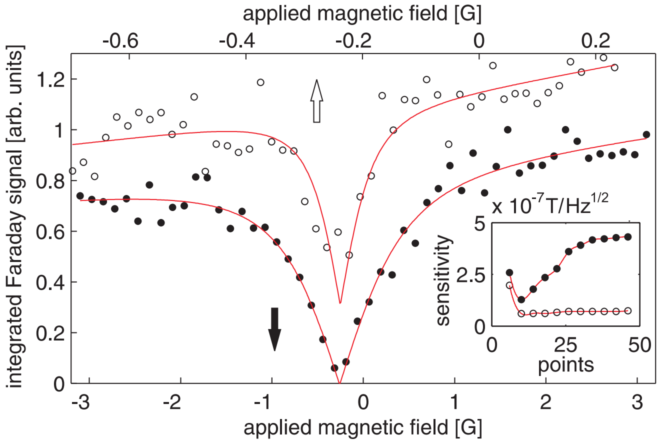

FIG. 3. Single-run magnetometry in an optical lattice. DFFI signal as a function of the applied magnetic field along the z-axis. Open circles: Magnetic field sweep over 0.93 G at $|\mathbf{B_r}| = 0.053$ G. Full dots: Magnetic field sweep over 6.2 G at $|\mathbf{B_r}| = 1.03$ G. The inset shows the sensitivity of the offset field extraction for the two realizations as a function of number of data included points (centered around the signal minimum). The sensitivity is estimated as the error of the fit times the square root of time taken to record the included data points.

to the scale of a single lattice site ($\approx 0.5\ \mu$m). We adapt the standard strategy of vapor cell magnetometers[22] by relying on time dependent control of additional magnetic bias fields to determine the magnetic field components.

To realize this lattice magnetometer, the atomic cloud is transferred into a 1D vertical lattice at a wavelength of 914 nm, whereupon we sweep the magnitude of an additional magnetic field applied along the z-axis. During this sweep, 50 DFFI pulses are taken to obtain the integrated Faraday signal at each applied magnetic field B_z as shown in Fig. 3 for two sweep widths and transverse magnetic fields. The data was normalized and fitted with $\mathrm{e}^{-\beta t}|B_z - B_{z_0}|/|\mathbf{B}|$, where the modulus is taken because our method is not sensitive to the sign of the Faraday rotation. The fit yields the offset field in the z-direction B_{z_0} and the magnitude of the transverse field $|\mathbf{B_r}|$. The exponential factor in the fit function accounts for atom loss during the sweep. In a first approach to quantify the sensitivity of such a time dependent vector magnetometer, the precision of extracting B_{z_0} was evaluated as a function of the number of included data points (Fig. 3 inset) yielding best values of $0.6 \cdot 10^{-7}\ \mathrm{T}/\sqrt{\mathrm{Hz}}$ for the smaller sweep. The sweeps yield an offset field $B_{z_0} = -0.252(13)$ G which is in agreement with our microwave calibration technique. This demonstration shows new avenues for magnetometry with DFFI, which could be better exploited with an optimized magnetometry sequence.

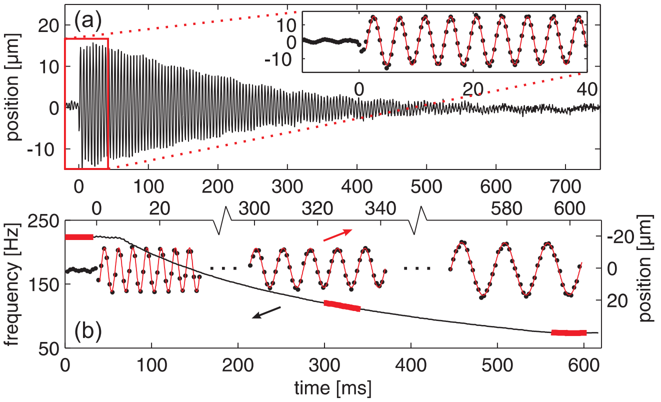

FIG. 4. Monitoring of spatial dynamics. a) Non-destructive measurement of the cloud position during a damped oscillation. b) Non-destructive measurement of the cloud position during a decompression of the magnetic trap. The cloud position and oscillation frequency are shown within three time intervals during the decompression.

Finally, DFFI allows for the non-destructive investigation of spatial dynamics. This is shown by monitoring the position of the atomic cloud as it oscillates in a harmonic potential. Since a single cloud can be probed repeatedly, one can map its trajectory in a single experimental sequence. This has previously been realized without spatial resolution to monitor breathing[27] and center-of-mass oscillations[28]; however, this approach fails for more complicated trajectories, e.g., when the position of the trapping potential is dynamically varied during the oscillation. Figure 4 a) shows the position of the cloud recorded in a single experiment by acquiring a total of 2000 images at intervals of 0.402 ms. Initially, a cloud of about 10^6 atoms at 1 μK was created in a magnetic trap and the imaging was started. Shortly afterwards ($t = 0$), the magnetic trap was turned off for a duration of 70 μs, which initiated a strong vertical oscillation. The initial part of the oscillation was fitted to obtain the trapping frequency of 222.44(6) Hz as shown in the inset of Fig. 4 a). The residual anharmonicity of the trap makes the system ergodic and slowly transfers the collective motion of the atoms into thermal energy. This results in a decrease of the oscillation amplitude and heating of the cloud which can be extracted from the DFFI pictures simultaneously.

This continuous probing of the spatial dynamics enables us to monitor dynamic changes of the system in a single sequence. To demonstrate this, we have observed an oscillating cloud during a decompression of the trap. Again, we prepared a cold cloud in a magnetic trap and started the acquisition of 750 images at intervals of 0.89 ms. The oscillations were initiated at time $t = 0$ and after a hold time of 60 ms we began to decrease the current of the magnetic trap and simultaneously increase the bias field. The resulting decrease in the trapping frequency caused the cloud to sag due to gravity while it continued to oscillate. By subtracting the shift of the equilibrium position we obtained the chirped oscillations; these oscillations were fitted within short time intervals to extract the time dependent trapping frequency, as shown in Fig. 4 b). These measurements highlight the advantages of spatially resolved non-destructive probing, since the temperature and the in-trap equilibrium position can not be extracted from non-spatially resolved dispersive methods[27,28].

In conclusion, we have demonstrated a simple and precise method to non-destructively probe ultracold atomic samples. This method can be implemented by inserting a polarizer into a standard absorption imaging system. We have investigated DFFI over a wide range of parameters and have shown it provides precise measurements of the atomic temperature and density. The potential of the method as a tool for the characterization and manipulation of ultra-cold atoms was demonstrated in three applications: Shot-to-shot atom number fluctuations were avoided, single-shot spatially resolved vector magnetometry in an optical lattice was performed, and the spatial dynamics of the system was monitored. In combination with fast data analysis, this method will allow for quantum engineering using measurements and feedback. In particular, it will be interesting to investigate if it can extend the methods for short-cuts to adiabaticity currently under investigation[29] and if it allows for the deterministic production of exotic quantum states.

We thank J. H. Müller for fruitful discussions. We acknowledge support from the Danish National Research Foundation, the Danish Council for Independent Research, and the Lundbeck Foundation.

[1] K. Hammerer, Rev. Mod. Phys. **82**, 1041–1093 (2010).
[2] W. Ketterle, D. S. Durfee, and D. M. Stamper-Kurn. In *Proceedings of the International School of Physics of Enrico Fermi,Course CXL: Bose-Einstein condensation in gases,* M. Inguscio, S. Stringari, and C. E. Wieman, editors, 67–164. Italian Physical Society, (1998).
[3] D. Budker, W. Gawlik, D. F. Kimball, S. M. Rochester, V. V. Yashchuk, and A. Weis, Rev. Mod. Phys. **74**, 1153–1201 (2002).
[4] L. Turner, K. Domen, and R. Scholten, Phys. Rev. A **72**, 031403 (2005).
[5] A. Ramanathan, S. R. Muniz, K. C. Wright, R. P. Anderson, W. D. Phillips, K. Helmerson, and G. K. Campbell, Rev. Sci. Instrum. **83**, 083119 (2012).
[6] B. Julsgaard, A. Kozhekin, and E. S. Polzik, Nature **413**, 400–403 (2001).
[7] B. Julsgaard, J. Sherson, J. I. Cirac, J. Fiurásek, and E. S. Polzik, Nature **432**, 482–6 (2004).
[8] J. F. Sherson, H. Krauter, R. K. Olsson, B. Julsgaard, K. Hammerer, I. Cirac, and E. S. Polzik, Nature **443**, 557–60 (2006).
[9] M. Kubasik, M. Koschorreck, M. Napolitano, S. de Echaniz, H. Crepaz, J. Eschner, E. S. Polzik, and M. W. Mitchell, Phys. Rev. A **79**, 043815 (2009).
[10] F. Kaminski, N. Kampel, M. Steenstrup, A. Griesmaier, E. Polzik, and J. Müller, Eur. Phys. J. D **66**, 1–8 (2012).
[11] T. Takano, M. Fuyama, R. Namiki, and Y. Takahashi, Phys. Rev. Lett. **102**, 033601 (2009).
[12] M. Vengalattore, J. M. Higbie, S. R. Leslie, J. Guzman, L. E. Sadler, and D. M. Stamper-Kurn, Phys. Rev. Lett. **98**, 200801 (2007).
[13] Y. Liu, S. Jung, S. Maxwell, L. Turner, E. Tiesinga, and P. Lett, Phys. Rev. Lett. **102**, 125301 (2009).
[14] U. Schünemann, H. Engler, R. Grimm, M. Weidemüller, and M. Zielonkowski, Rev. Sci. Instrum. **70**, 242–243 (1999).
[15] S. J. Park, H. K. Andersen, S. Mai, J. Arlt, and J. F. Sherson, Phys. Rev. A **85**, 033626 (2012).
[16] T. Yefsah, R. Desbuquois, L. Chomaz, K. Günter, and J. Dalibard, Phys. Rev. Lett. **107**, 130401 (2011).
[17] G. Reinaudi, T. Lahaye, Z. Wang, and D. Guéry-Odelin, Opt. Lett. **32**, 3143–3145 (2007).
[18] J. Roberts, N. Claussen, S. Cornish, and C. Wieman, Phys. Rev. Lett. **85**, 728–31 (2000).
[19] C. McKenzie, J. Hecker Denschlag, H. Häffner, A. Browaeys, L. E. E. de Araujo, F. K. Fatemi, K. M. Jones, J. E. Simsarian, D. Cho, A. Simoni, E. Tiesinga, P. S. Julienne, K. Helmerson, P. D. Lett, S. L. Rolston, and W. D. Phillips, Phys. Rev. Lett. **88**, 120403 (2002).
[20] D. Budker and M. Romalis, Nature Physics **3**, 227–234 (2007).
[21] I. K. Kominis, T. W. Kornack, J. C. Allred, and M. V. Romalis, Nature **422**, 596–9 (2003).
[22] S. J. Seltzer and M. V. Romalis, Appl. Phys. Lett. **85**, 4804 (2004).
[23] S. Wildermuth, S. Hofferberth, I. Lesanovsky, S. Groth, P. Krüger, J. Schmiedmayer, and I. Bar-Joseph, Appl. Phys. Lett. **88**, 264103 (2006).
[24] F. K. Fatemi and M. Bashkansky, Optics express **18**, 2190–6 (2010).
[25] A. Smith, B. E. Anderson, S. Chaudhury, and P. S. Jessen, J. Phys. B: At. Mol. Opt. Phys. **44**, 205002 (2011).
[26] M. Koschorreck, M. Napolitano, B. Dubost, and M. W. Mitchell, Appl. Phys. Lett. **98**, 074101 (2011).
[27] P. G. Petrov, D. Oblak, C. L. G. Alzar, N. Kjærgaard, and E. S. Polzik, Phys. Rev. A **75**, 033803 (2007).
[28] M. Kohnen, P. G. Petrov, R. A. Nyman, and E. A. Hinds, New J. Phys. **13**, 085006 (2011).
[29] J.-F. Schaff, X.-L. Song, P. Capuzzi, P. Vignolo, and G. Labeyrie, EPL (Europhysics Letters) **93**, 23001 (2011).